THE GEOLOGICAL SOCIETY OF AMERICA®

Alternating Southern and Northern Hemisphere climate response to astronomical forcing during the past 35 m.y.

David De Vleeschouwer[1]*, Maximilian Vahlenkamp[1], Michel Crucifix[2,3], and Heiko Pälike[1]
[1]MARUM Center for Marine Environmental Science, Universität Bremen, Leobener Strasse, D-28359 Bremen, Germany
[2]Université catholique de Louvain, Earth and Life Institute, 1, Place de l'Université, B-1348 Louvain-la-Neuve, Belgium
[3]Belgian National Fund for Scientific Research, 5, Rue d'Egmont, B-1000 Brussels, Belgium

ABSTRACT

Earth's climate has undergone different intervals of gradual change as well as abrupt shifts between climate states. Here we aim to characterize the corresponding changes in climate response to astronomical forcing in the icehouse portion of the Cenozoic, from the latest Eocene to the present. As a tool, we use a 35-m.y.-long $\delta^{18}O_{benthic}$ record compiled from different high-resolution benthic isotope records spliced together (what we refer to as a megasplice).We analyze the climate response to astronomical forcing during four 800-k.y.-long time windows. During the mid-Miocene Climatic Optimum (ca. 15.5 Ma), global climate variability was mainly dependent on Southern Hemisphere summer insolation, amplified by a dynamic Antarctic ice sheet; 2.5 m.y. later, relatively warm global climate states occurred during maxima in both Southern Hemisphere and Northern Hemisphere summer insolation. At that point, the Antarctic ice sheet grew too big to pulse on the beat of precession, and the Southern Hemisphere lost its overwhelming influence on the global climate state. Likewise, we juxtapose response regimes of the Miocene (ca. 19 Ma) and Oligocene (ca. 25.5 Ma) warming periods. Despite the similarity in $\delta^{18}O_{benthic}$ values and variability, we find different responses to precession forcing. While Miocene warmth occurs during summer insolation maxima in both hemispheres, Oligocene global warmth is consistently triggered when Earth reaches perihelion in the Northern Hemisphere summer. This pattern is in accordance with previously published paleoclimate modeling results, and suggests an amplifying role for Northern Hemisphere sea ice.

INTRODUCTION

Hays et al. (1976, p. 1121) conclusively identified astronomical insolation forcing as the so-called "pacemaker of the Ice Ages." From then on, deciphering the imprint of astronomical climate forcing in geologic archives of past climates became an indispensable part of paleoclimatology and paleoceanography (Hinnov and Hilgen, 2012). Astronomical-scale climatic changes are recorded in $\delta^{18}O$ of foraminiferal calcite tests. The $\delta^{18}O$ of benthic foraminifer tests reflects a combination of temperature state and size of Earth's cryosphere at the time of their formation. These characteristics motivated the construction of the Pliocene–Pleistocene $\delta^{18}O_{benthic}$ stack of Lisiecki and Raymo (2005; LR04, http://www.lorraine-lisiecki.com/stack.html), as well as several $\delta^{18}O_{benthic}$ compilations (Cramer et al., 2009; Friedrich et al., 2012; Zachos et al., 2001, 2008). A stack is an average of different, coeval $\delta^{18}O_{benthic}$ records, placed on a common age model, whereas a compilation is a collection of records, all in the time domain, but with their separate age models. In this study we apply a different approach to integrate paleoclimate information from globally distributed $\delta^{18}O_{benthic}$ records. We constructed a 35-m.y.-long $\delta^{18}O_{benthic}$ megasplice (Fig. 1C) of different high-resolution benthic isotope records (see the GSA Data Repository[1] for details). In contrast to existing compilations and stacks that respectively mix and average time-equivalent data across sites, the megasplice comprises data from a single site at any point in time, allowing analyses that require a high-resolution record at astronomical resolution.

Visualizing Different Astronomical Rhythms Using a Gaussian Process

The megasplice provides a novel stratigraphic tool that is suitable as a global framework for orbital-scale correlation of paleoclimate records. Here we quantify and visualize the changing paleoclimate response to astronomical forcing (i.e., different astronomical rhythms) throughout geologic time. The wavelet spectrograms in Figures 1A and 1B show a remarkable transition from a $\delta^{18}O_{benthic}$ signal dominated by eccentricity-modulated precession to an obliquity-driven signal after the mid-Miocene climatic transition (MMCT). In this paper, we focus on the $\delta^{18}O_{benthic}$ response to astronomical forcing in four specific intervals: the MMCT, the mid-Miocene climatic optimum (MMCO), and the early Miocene and late Oligocene warming intervals. We calculate $\delta^{18}O_{benthic}$ response surfaces in a three-dimensional space spanned by obliquity and eccentricity-modulated precession (Figs. 2 and 3) within 800-k.y.-long time windows (Figs. 1A, 1B). The underlying statistical model is a Gaussian process (see the Data Repository) that renders the dependence of one variable, here $\delta^{18}O_{benthic}$, in a multidimensional space. Gaussian processes are routinely used for geospatial interpolation (i.e., kriging; Cressie, 1993).

The methodology would be susceptible to circular reasoning if $\delta^{18}O_{benthic}$ records were densely tuned to obliquity and precession. To alleviate this issue, we preserved only one tie point between depth and time every ~100 k.y., so that the phase relationship between astronomical forcing and $\delta^{18}O_{benthic}$ can be evaluated independently. The four time windows discussed herein all utilize data from the equatorial Pacific (Ocean Drilling Program Sites 1137, 1138, and 1218), thus avoiding complications when comparing astronomical imprints across oceans or latitudes.

The $\delta^{18}O_{benthic}$ response surfaces (Figs. 2 and 3) show heavy to light $\delta^{18}O_{benthic}$ values as a function of the astronomical configuration. Blue to red colors designate cooler to warmer global climates as well as higher to lower global ice volume. The steps between different colors are fixed to 0.02‰, so that variability can be compared among different time windows. The $\delta^{18}O_{benthic}$ gradients in Figures 2B, 2E, 3B, and 3E reveal the relative imprint of obliquity and precession. Figure 2E, for example, has a steep gradient along the *y* axis, indicating that the corresponding climate system was responding more strongly to eccentricity-modulated precession ($e \cdot \sin\tilde{\omega}$; e is eccentricity and $\tilde{\omega}$ is the longitude

*E-mail: ddevleeschouwer@marum.de

[1]GSA Data Repository 2017107, detailed description of the construction of the megasplice, details and evaluation of the Gaussian process, and the R-code to generate Figures 2 and 3, is available online at http://www.geosociety.org/datarepository/2017/ or on request from editing@geosociety.org. The megasplice dataset is available on PANGAEA at doi:10.1594/PANGAEA.869815.

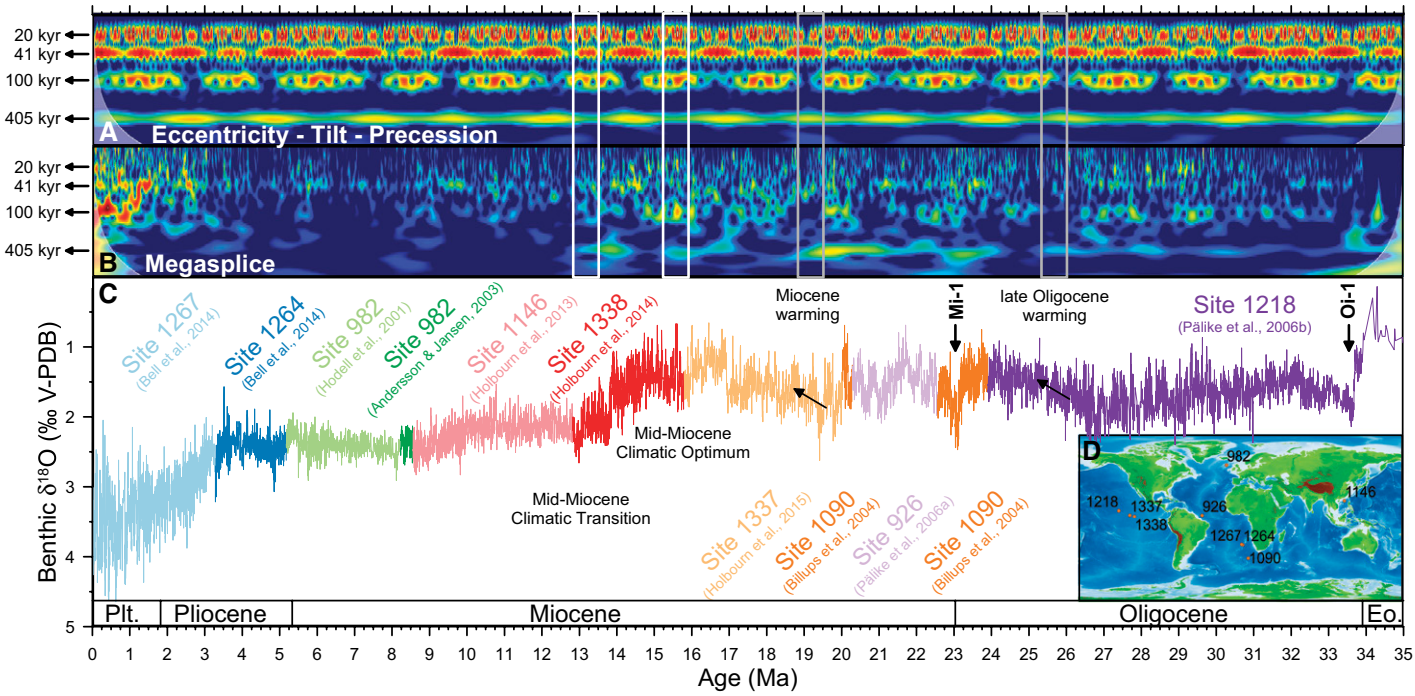

Figure 1. Benthic δ¹⁸O megasplice. A, B: Wavelet spectrograms of an eccentricity-tilt-precession composite (Laskar et al., 2004) and the benthic δ¹⁸O megasplice visualize changes in the paleoclimate response to astronomical forcing. C: The megasplice consists of nine globally distributed benthic oxygen isotope records: IODP–ODP (Integrated Ocean Drilling Program–Ocean Drilling Program) Sites 1267 and 1264 (Bell et al., 2014), Site 982 (Andersson and Jansen, 2003; Hodell et al., 2001), Site 1146 (Holbourn et al., 2013), Site 1338 (Holbourn et al., 2014), Site 1337 (Holbourn et al., 2015), Site 1090 (Billups et al., 2004), Site 926 (Pälike et al., 2006a), and Site 1218 (Pälike et al., 2006b). A version of this figure without labels is available as Figure DR1 (see footnote 1). Plt.—Pleistocene; Eo—Eocene; V-PDB—Vienna Peedee belemnite.

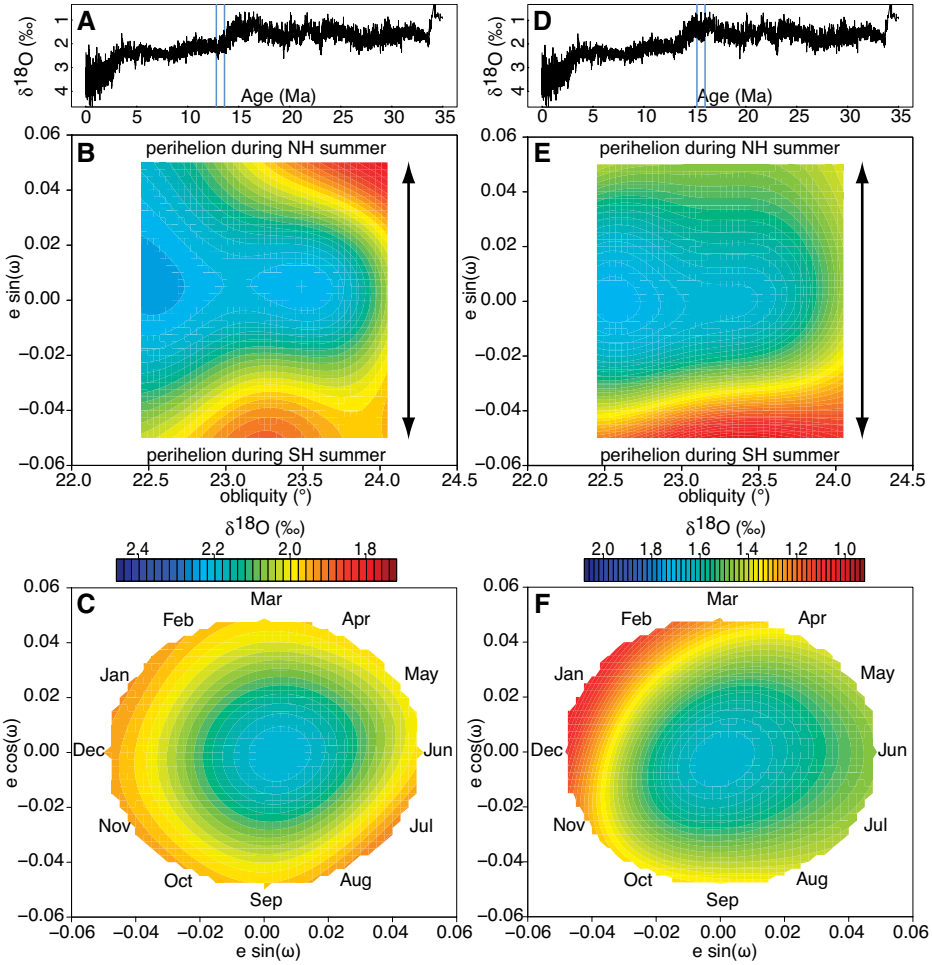

Figure 2. Benthic δ¹⁸O response to astronomical forcing between 13.6 and 12.8 Ma (left panels: mid-Miocene climatic transition), and between 16 and 15.2 Ma (right panels: mid-Miocene Climatic Optimum). Blue to red colors designate heavy to light $\delta^{18}O_{benthic}$ values, and thus indicate cooler to warmer global climates as well as higher to lower global ice volume. The $e \cdot \sin\tilde{\omega}$ obliquity plots represent a slice at $e \cdot \cos\tilde{\omega} = 0$, while the $e \cdot \sin\tilde{\omega} - e \cdot \cos\tilde{\omega}$ plots show the dependency of $\delta^{18}O_{benthic}$, averaged over the distribution of obliquity (e is eccentricity and $\tilde{\omega}$ is the longitude of perihelion measured from the spring equinox; see text). NH—Northern Hemisphere; SH—Southern Hemisphere.

of perihelion measured from the spring equinox) than to obliquity. However, detailed insight into how the climate system responded to changes in eccentricity and precession is provided in Figures 2C, 2F, 3C, and 3F. These figures should be read as polar plots, for which the azimuth represents $\tilde{\omega}$ and the radius represents e (the center represents e = 0). The month during which Earth reaches perihelion is indicated at the corresponding azimuth. Figure 2F thus represents a climate that is warmest when the Earth is in perihelion at January, under high eccentricity. We provide a well-known example in Figure DR3 in the Data Repository, in which we compare the astronomical rhythms of the 100 k.y. world (0.8–0 Ma) and the obliquity world (1.8–1.0 Ma).

RESULTS AND DISCUSSION

Contrasting Miocene Rhythms

The response of $\delta^{18}O_{benthic}$ to astronomical forcing between 13.6 and 12.8 Ma is shown in Figures 2A–2C. This time window covers the first 800 k.y. after the MMCT (Fig. 1) and thus represents a climate state with an expanded East Antarctic ice sheet (Flower and Kennett, 1994; Wright et al., 1992). Figures 2D–2F show the $\delta^{18}O_{benthic}$ response between 16 and 15.2 Ma, a time slice that corresponds to the culmination of the MMCO (Fig. 1). During this relatively warm period, Antarctic ice sheets were much smaller than today and presumably more dynamic (Fielding et al., 2011; Griener et al., 2015; Passchier et al., 2013; Warny et al., 2009). A large difference in East Antarctic ice volume thus exists between the two time windows depicted in Figure 2. Nevertheless, the $\delta^{18}O_{benthic}$ response to obliquity is similar for both time windows, with isotopic values becoming lighter with increasing obliquity (Figs. 2B and 2E). The response to climatic precession ($e \cdot \sin\tilde{\omega}$), however, differs markedly between the two time windows (Figs. 2C, 2F). The MMCO is a period with a low global ice volume and the isotopic response to eccentricity-modulated precession is intense; the lightest $\delta^{18}O_{benthic}$ values occur when eccentricity is high and Earth reaches perihelion in January (Fig. 2F). The heaviest isotope values occur at low eccentricity. In the MMCT time slice (13.6–12.8 Ma), the isotopic response to precession is bimodal, with lighter $\delta^{18}O_{benthic}$ values when perihelion is reached in either July or January (Fig. 2C). These significantly different responses to precession portray the effect of a highly dynamic continental ice sheet. During the MMCO, the Northern Hemisphere was free of continental ice sheets, while the Antarctic ice sheet was smaller but more dynamic than it is today. Antarctic ice cover and global climate, represented by $\delta^{18}O_{benthic}$, mainly depended on Southern Hemisphere summer insolation, with minimum Antarctic ice volume and peak warmth when Southern Hemisphere summer insolation

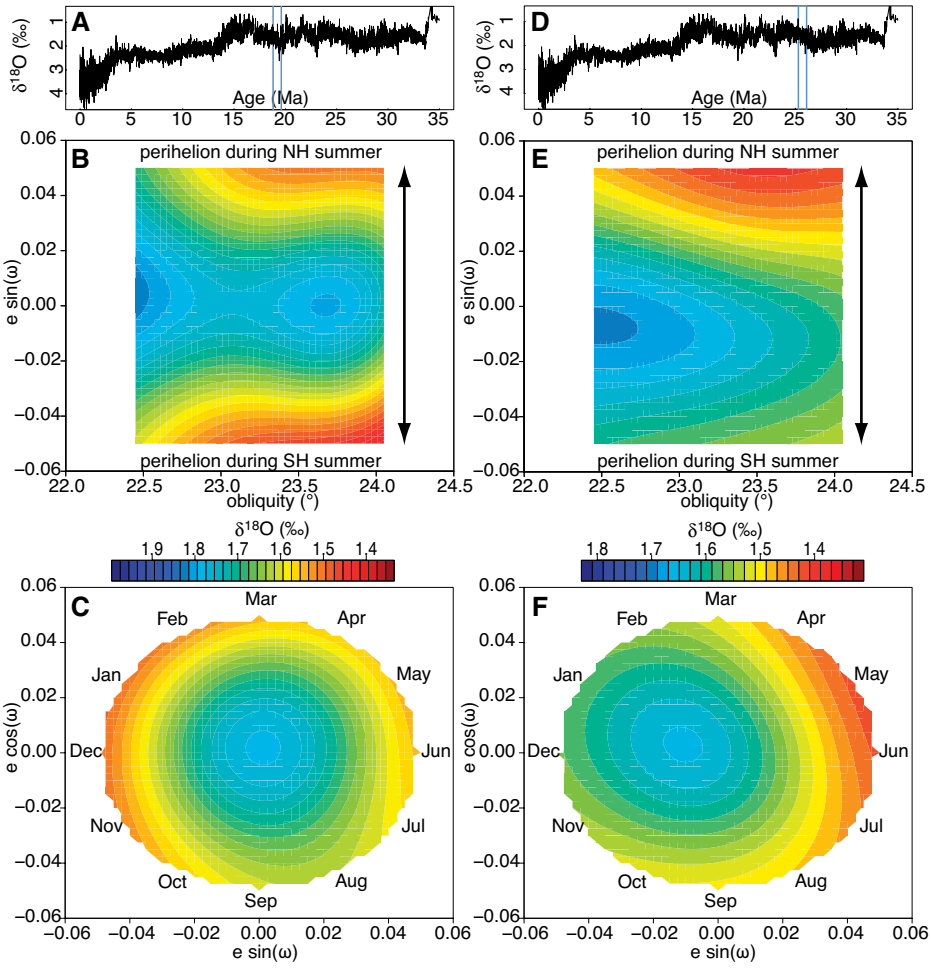

Figure 3. Benthic $\delta^{18}O$ response to astronomical forcing between 19.6 and 18.8 Ma (left panels, early Miocene warming), and between 26.1 and 25.3 Ma (right panels, late Oligocene warming). NH—Northern Hemisphere; SH—Southern Hemisphere; e is eccentricity and $\tilde{\omega}$ is the longitude of perihelion measured from the spring equinox; see text).

was maximum, i.e., perihelion in January (Fig. 2F). After extensive ice growth over Antarctica ca. 13.8 Ma, this ice sheet grew too big to pulse on the beat of precession, and thereby lost its overwhelming influence on the global climate state. At the same time, the influence of the Northern Hemisphere was growing. For example, through ice-albedo feedback mechanisms, which became more important in the cooling Arctic region (Darby, 2008; Krylov et al., 2008; Stein et al., 2016). The combined effect of a less dynamic Antarctic ice sheet and a dynamic Arctic cryosphere explains the bimodal precession response between 13.6 and 12.8 Ma (MMCT; Fig. 2C).

Different Warming Regimes During the Oligocene and Miocene

We compare here two intervals of long-term warming. The younger time slice (19.6–18.8 Ma; Figs. 3A–3C) corresponds to the warming that eventually culminated in the MMCO; the older time slice coincides with the latest Oligocene warming (Pälike et al., 2006b) (26.1–25.3 Ma; Figs. 3D–3F). Based on the absolute $\delta^{18}O_{benthic}$ values and their variability, one might expect similar climate response dynamics. Broadly speaking, this is what the surface response plots show, with cooler global climate (heavy $\delta^{18}O_{benthic}$) under low eccentricity and low obliquity (Figs. 3B, 3C, 3E, 3F). Nonetheless, we observe an important difference in the response to precession between the Miocene and Oligocene warming. Whereas the Miocene time slice shows a symmetrical and bimodal $\delta^{18}O_{benthic}$ response to precession (Fig. 3C), Oligocene global warmth consistently occurs when Earth reaches perihelion in May or June (Fig. 3F). The late Oligocene response is consistent with an amplification of a Northern Hemisphere summer insolation signal through a vigorous feedback mechanism. This is remarkable, considering that during the Oligocene, continental ice in the Arctic was probably limited to no more than a few isolated glaciers (Eldrett et al., 2007; Pekar et al., 2006). Arctic sea ice, however, may have played a central role in positive feedback mechanisms, through its albedo as well as through its effect on deep-water formation and ocean conveyor circulation. At the same time in the Southern Hemisphere, the Antarctic continent was still

heavily glaciated. For the 26.1–25.3 Ma window considered here, Pekar et al. (2006) estimated an ice volume equivalent to 75%–100% of the present-day East Antarctic ice sheet, too large to respond on a precessional time scale. Meanwhile, climate modeling results by Eldrett et al. (2009) for the Arctic show a strong decrease in Arctic winter temperatures across the Eocene-Oligocene transition, with the formation of thick large-scale winter sea ice. Given this general stage of the Oligocene climate system, we suggest that the $\delta^{18}O_{benthic}$ response to precession (Fig. 3F) reflects the accelerated melting of sea ice in spring and early summer, when insolation is high during those seasons. This regional response to astronomical forcing is then propagated to global climate through multiple positive feedback mechanisms (e.g., ice albedo, deep-water formation). This interpretation is reinforced by the fact that minimum $\delta^{18}O_{benthic}$ occurs when the Earth reaches perihelion in May, i.e., the month during which sea-ice volume starts to decline.

CONCLUSIONS

This paper documents four different ways in which the global climate system responds to astronomical insolation forcing from the latest Eocene to the present. Shifts in key boundary conditions like continental distribution, pCO_2, or the size and distribution of the cryosphere thus had a significant influence on climate sensitivity to astronomical forcing. The presence of a dynamic cryosphere in the Southern or Northern Hemisphere seems to exert the principal control on the response of global climate to astronomical forcing in the icehouse of the past 35 m.y. We report an alternation of the driving hemisphere from the Northern Hemisphere during the late Oligocene, to the Southern Hemisphere during the MMCO, and back to the Northern Hemisphere during the Quaternary. The intermediate time slices (early Miocene and MMCT) exhibit a bimodal response to precession and thus suggest a balanced influence of both hemispheres on global climate.

ACKNOWLEDGMENTS

This work was funded by European Research Council Consolidator Grant EarthSequencing (grant agreement 617462).

REFERENCES CITED

Andersson, C., and Jansen, E., 2003, A Miocene (8–12 Ma) intermediate water benthic stable isotope record from the northeastern Atlantic, ODP Site 982: Paleoceanography, v. 18, 1013, doi:10.1029/2001PA000657.

Bell, D.B., Jung, S.J.A., Kroon, D., Lourens, L.J., and Hodell, D.A., 2014, Local and regional trends in Plio-Pleistocene $\delta^{18}O$ records from benthic foraminifera: Geochemistry, Geophysics, Geosystems, v. 15, p. 3304–3321, doi:10.1002/2014GC005297.

Billups, K., Pälike, H., Channell, J.E.T., Zachos, J.C., and Shackleton, N.J., 2004, Astronomic calibration of the late Oligocene through early Miocene geomagnetic polarity time scale: Earth and Planetary Science Letters, v. 224, p. 33–44, doi:10.1016/j.epsl.2004.05.004.

Cramer, B.S., Toggweiler, J.R., Wright, J.D., Katz, M.E., and Miller, K.G., 2009, Ocean overturning since the Late Cretaceous: Inferences from a new benthic foraminiferal isotope compilation: Paleoceanography, v. 24, PA4216, doi:10.1029/2008PA001683.

Cressie, N., 1993, Statistics for spatial data: Wiley Series in Probability and Statistics Volume 298: Chichester, UK, John Wiley & Sons, 900 p.

Darby, D.A., 2008, Arctic perennial ice cover over the last 14 million years: Paleoceanography, v. 23, PA1S07, doi:10.1029/2007PA001479.

Eldrett, J.S., Harding, I.C., Wilson, P.A., Butler, E., and Roberts, A.P., 2007, Continental ice in Greenland during the Eocene and Oligocene: Nature, v. 446, p. 176–179, doi:10.1038/nature05591.

Eldrett, J.S., Greenwood, D.R., Harding, I.C., and Huber, M., 2009, Increased seasonality through the Eocene to Oligocene transition in northern high latitudes: Nature, v. 459, p. 969–973, doi:10.1038/nature08069.

Fielding, C.R., Browne, G.H., Field, B., Florindo, F., Harwood, D.M., Krissek, L.A., Levy, R.H., Panter, K.S., Passchier, S., and Pekar, S.F., 2011, Sequence stratigraphy of the ANDRILL AND-2A drillcore, Antarctica: A long-term, ice-proximal record of Early to Mid-Miocene climate, sea-level and glacial dynamism: Palaeogeography, Palaeoclimatology, Palaeoecology, v. 305, p. 337–351, doi:10.1016/j.palaeo.2011.03.026.

Flower, B.P., and Kennett, J.P., 1994, The middle Miocene climatic transition: East Antarctic ice sheet development, deep ocean circulation and global carbon cycling: Palaeogeography, Palaeoclimatology, Palaeoecology, v. 108, p. 537–555, doi:10.1016/0031-0182(94)90251-8.

Friedrich, O., Norris, R.D., and Erbacher, J., 2012, Evolution of middle to Late Cretaceous oceans—A 55 m.y. record of Earth's temperature and carbon cycle: Geology, v. 40, p. 107–110, doi:10.1130/G32701.1.

Griener, K.W., Warny, S., Askin, R., and Acton, G., 2015, Early to middle Miocene vegetation history of Antarctica supports eccentricity-paced warming intervals during the Antarctic icehouse phase: Global and Planetary Change, v. 127, p. 67–78, doi:10.1016/j.gloplacha.2015.01.006.

Hays, J.D., Imbrie, J., and Shackleton, N.J., 1976, Variations in the Earth's orbit: Pacemaker of the ice ages: Science, v. 194, p. 1121–1132, doi:10.1126/science.194.4270.1121.

Hinnov, L., and Hilgen, F., 2012, Cyclostratigraphy and astrochronology, *in* Gradstein, F.M., et al., eds., The geologic time scale 2012: Amsterdam, Elsevier, p. 63–83, doi:10.1016/B978-0-444-59425-9.00004-4.

Hodell, D.A., Curtis, J.H., Sierro, F.J., and Raymo, M.E., 2001, Correlation of Late Miocene to Early Pliocene sequences between the Mediterranean and North Atlantic: Paleoceanography, v. 16, p. 164–178, doi:10.1029/1999PA000487.

Holbourn, A., Kuhnt, W., Clemens, S., Prell, W., and Andersen, N., 2013, Middle to late Miocene stepwise climate cooling: Evidence from a high-resolution deep water isotope curve spanning 8 million years: Paleoceanography, v. 28, p. 688–699, doi:10.1002/2013PA002538.

Holbourn, A., Kuhnt, W., Lyle, M., Schneider, L., Romero, O., and Andersen, N., 2014, Middle Miocene climate cooling linked to intensification of eastern equatorial Pacific upwelling: Geology, v. 42, p. 19–22, doi:10.1130/G34890.1.

Holbourn, A., Kuhnt, W., Kochhann, K.G.D., Andersen, N., and Meier, K.J.S., 2015, Global perturbation of the carbon cycle at the onset of the Miocene Climatic Optimum: Geology, v. 43, p. 123–126, doi:10.1130/G36317.1.

Krylov, A.A., Andreeva, I.A., Vogt, C., Backman, J., Krupskaya, V.V., Grikurov, G.E., Moran, K., and Shoji, H., 2008, A shift in heavy and clay mineral provenance indicates a middle Miocene onset of a perennial sea ice cover in the Arctic Ocean: Paleoceanography, v. 23, PA1S06, doi:10.1029/2007PA001497.

Laskar, J., Robutel, P., Joutel, F., Gastineau, M., Correia, A., and Levrard, B., 2004, A long-term numerical solution for the insolation quantities of the Earth: Astronomy & Astrophysics, v. 428, p. 261–285, doi:10.1051/0004-6361:20041335.

Lisiecki, L.E., and Raymo, M.E., 2005, A Pliocene-Pleistocene stack of 57 globally distributed benthic $\delta^{18}O$ records: Paleoceanography, v. 20, PA1003, doi:10.1029/2004PA001071.

Pälike, H., Frazier, J., and Zachos, J.C., 2006a, Extended orbitally forced palaeoclimatic records from the equatorial Atlantic Ceara Rise: Quaternary Science Reviews, v. 25, p. 3138–3149, doi:10.1016/j.quascirev.2006.02.011.

Pälike, H., Norris, R.D., Herrle, J.O., Wilson, P.A., Coxall, H.K., Lear, C.H., Shackleton, N.J., Tripati, A.K., and Wade, B.S., 2006b, The heartbeat of the Oligocene climate system: Science, v. 314, p. 1894–1898, doi:10.1126/science.1133822.

Passchier, S., Falk, C.J., and Florindo, F., 2013, Orbitally paced shifts in the particle size of Antarctic continental shelf sediments in response to ice dynamics during the Miocene climatic optimum: Geosphere, v. 9, p. 54–62, doi:10.1130/GES00840.1.

Pekar, S.F., DeConto, R.M., and Harwood, D.M., 2006, Resolving a late Oligocene conundrum: Deep-sea warming and Antarctic glaciation: Palaeogeography, Palaeoclimatology, Palaeoecology, v. 231, p. 29–40, doi:10.1016/j.palaeo.2005.07.024.

Stein, R., et al., 2016, Evidence for ice-free summers in the late Miocene central Arctic Ocean: Nature Communications, v. 7, 11148, doi:10.1038/ncomms11148.

Warny, S., Askin, R.A., Hannah, M.J., Mohr, B.A.R., Raine, J.I., Harwood, D.M., Florindo, F., and Team, T.S.S., 2009, Palynomorphs from a sediment core reveal a sudden remarkably warm Antarctica during the middle Miocene: Geology, v. 37, p. 955–958, doi:10.1130/G30139A.1.

Wright, J.D., Miller, K.G., and Fairbanks, R.G., 1992, Early and Middle Miocene stable isotopes: Implications for deepwater circulation and climate: Paleoceanography, v. 7, p. 357–389, doi:10.1029/92PA00760.

Zachos, J.C., Pagani, M., Sloan, L., Thomas, E., and Billups, K., 2001, Trends, rhythms, and aberrations in global climate 65 Ma to present: Science, v. 292, p. 686–693, doi:10.1126/science.1059412.

Zachos, J.C., Dickens, G.R., and Zeebe, R.E., 2008, An early Cenozoic perspective on greenhouse warming and carbon-cycle dynamics: Nature, v. 451, p. 279–283, doi:10.1038/nature06588.

Manuscript received 7 October 2016
Revised manuscript received 23 December 2016
Manuscript accepted 28 December 2016

Printed in USA